

Natural cooling of stand-alone houses using solar chimney and evaporative cooling cavity

M. Maerefat*, A.P. Haghighi

Mech. Eng. Department, Faculty of Engineering, Tarbiat Modares University, Tehran 14115-143, Iran

ARTICLE INFO

Article history:

Received 24 December 2008

Accepted 4 February 2010

Available online 26 February 2010

Keywords:

Passive cooling

Solar chimney

Evaporative cooling cavity

ABSTRACT

In this study a low-energy-consumption technique to enhance passive cooling and natural ventilation in a solar house, using a system consisting of a Solar Chimney (SC) and an Evaporative Cooling Cavity (ECC) has been proposed. The capability of the system to meet the required thermal needs of individuals and the effects of main geometric parameters on the system performance has been studied. The dependence of the system performance on outdoor air temperature has been studied to determine the operative conditions for appropriate effectiveness, regarding thermal comfort criteria. To determine the heat and mass transfer characteristics of the system, a mathematical model based on conservation equations of mass and energy has been developed and solved by an iterative method. The findings show that the system is capable of providing good indoor air condition at daytime in a living room, even with poor solar intensity of 200 W/m^2 . The results show that when the relative humidity is lower than 50%, the system can make good indoor air condition even at 40°C , and a higher performance is achieved using ECC with cocurrent configuration. It is found that the proposed system may be applied successfully in hot arid climates to fulfill the indoor thermal comfort expectations.

© 2010 Elsevier Ltd. All rights reserved.

1. Introduction

Providing good indoor conditions become problematic when outdoor temperature is high. The most effective method to cool a building is to avoid heating. The basic source of heat in a building is the sunlight energy absorbed through the roof, walls, windows as well as the heat generated by appliances and air leakages. Although, there are some specific methods to prevent the accumulation of heat, adopting all those strategies might not be possible or adequate. Air-conditioning provides some relief. However, its initial costs as well as the related costs of electricity consumption make it an expensive technology to afford. In addition, conventional air-conditioners use refrigerants made of chlorine compounds which are unfortunately involved in depletion of the ozone layer and global warming. It is noteworthy that human production of greenhouse gases, especially CO_2 , is changing the global climate. Statistics show that nearly 50% of CO_2 emissions in developed countries are derived from energy consumption in the buildings. Thus, it is obvious that the well-controlled and energy-efficient ventilation systems are prerequisite for low-energy-consumption as well as a substantial reduction in CO_2 emissions.

Employing natural or passive cooling system can be an alternative way to maintain a cool house or reduce air-conditioning load. A passive cooling system employs non-mechanical procedures to maintain suitable indoor temperature. Ingenuity of ancient architectures has showed how a rational use of traditional passive techniques, along with a smart design, was involved in having desired summer comfort without a need to pursue mechanical cooling systems. Recently, there is much inclination toward these systems, especially due to economic and environmental reasons.

This study attempts to present a new low-energy passive technique to ventilate and provide thermal needs of occupants in the buildings. Here, the solar energy and an evaporative cooling technique are used simultaneously. Many researches have been conducted on using natural ventilation and evaporative cooling for producing cool air so far. First of all, Bahadori introduced the idea of capturing the wind within a wind tower and then passing it through wetted conduit walls [1]. Verma et al. studied numerically the performance of a passive cooling system which uses evaporative cooling technique on the roof. They concluded that this method is an effective technique which significantly reduces air temperature of the room [2]. Giabaklou and Ballinger presented another method of cooling in low-rise multi-storey buildings through a simple water cascade associated with openings and balconies of individual units to provide a passive cooling. This system applies the evaporative cooling technique to reduce ambient air temperature by passing air

* Corresponding author. Tel.: +98 21 8288 3360; fax: +98 21 8288 3381.
E-mail address: maerefat@modares.ac.ir (M. Maerefat).

over the water falling film [3]. Aboulnaga analytically studied the roof solar chimney coupled with wind cooled cavity to obtain the best performance of the system [4]. Raman et al. described two passive models for the summer cooling system. The first model consisting of two solar chimneys: one placed on the roof to ventilate the room air and the other on the ground adjacent to the room to act as an evaporative cooler during summer. The second model consisting of a south wall collector and a roof duct is cooled from the top by a sack of cloth evaporative cooling system. The results showed that thermal performance of the second model is better than the first one [5]. Manzan and Saro studied a passive system consisting of a ventilated roof with a wet lower surface of the cavity which flows the external air. They investigated thermal performance of the system by numerical modeling of evaporative cooling process through the chimney [6]. Dai et al. presented a new passive cooling system for humid climate using the solar chimney and adsorption cooling system. Its performance was investigated based on a mathematical model. The system increases the rate of ventilation and provides the cooling without increasing humidity of the room [7]. Chungloo and Limmeechokchai experimentally investigated the performance of a passive cooling consisting of a solar chimney and water spraying system that was placed on the roof under hot and humid climate. They reported that the system performed well in high ambient temperature [8].

The review of the related literature shows that the combination of both a solar chimney and an evaporative cooling which provides natural ventilation together with temperature reduction inside a building has not been investigated yet. This ventilation system has the merits of being environmentally friendly and energy saving at the same time.

Fig. 1 illustrates a schematic plan of the system consisting of two parts: a solar chimney and a cooling cavity. The solar chimney comprises a glass surface oriented to the south where the solar radiation crosses through an absorber wall which acts as a capturing surface.

In the cooling cavity, circulating water is sprayed onto the top of the wall where it flows as a thin film along the wall surfaces of the air passage. The air, near the water film, is at an average temperature of the water spray film. Since partial pressure of water vapor at the interface is higher than air pressure, there is a mass transfer of evaporated water into the air. This is associated with a latent heat transfer and water vaporization. At the same time, convective heat transfer takes place due to the temperature difference between surface of the water and the air. At the end of evaporation process, the cooled falling water is collected in a basin that is provided at the bottom of the evaporative cavity. This water is recycled again to the sprinkler by means of a pump. The water finally achieves an adiabatic saturation temperature of the air naturally after several circulations. Thus we can call it a direct evaporative passive cooling system.

The system operates as follows: the solar energy heats up the room air flowing through the chimney, and the hot air generates the draft in the chimney. This draft induces air ventilation in the whole system: solar chimney, room, and cooling cavity. The chimney effect causes the air to be drawn through the cooling cavity with wetted cool surfaces and to remove heat from this air and brings cooled supply air into the room. Therefore, both cooling and ventilation are provided during daytime by solar energy.

The present work intends to investigate the capability of the proposed system to provide thermal comfort condition in a living room. Therefore, the system is modeled and solved and the obtained indoor thermal condition is checked against the Adapted Comfort Standard (ACS) specified for thermal comfort in naturally ventilated buildings. The adapted comfort standard is shown in Fig. 2 which is drawn based on data reported by Ref. [9]. The ACS only gives the acceptable temperature range of indoor air when the outdoor temperature is within the range of 0–40 °C and does not recommend the suitable rate of ventilation. However, the ventilation rate is set approximately around 3 air changes per hour to reduce possible pollution concentration and to ensure that the thermal comfort condition is provided.

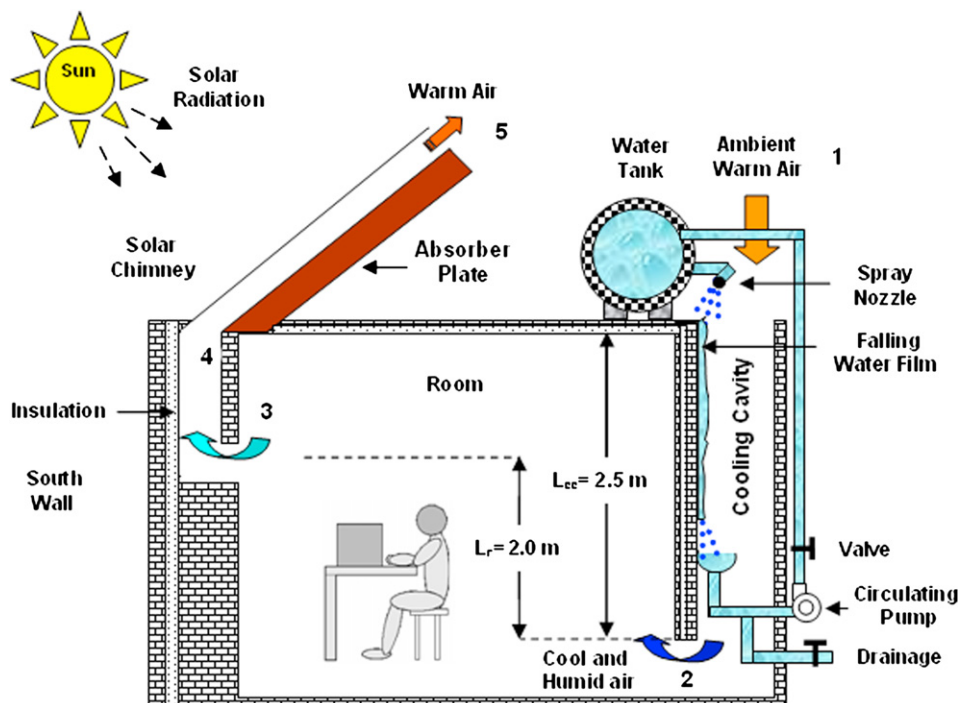


Fig. 1. Schematic diagram of solar chimney and cooling cavity.

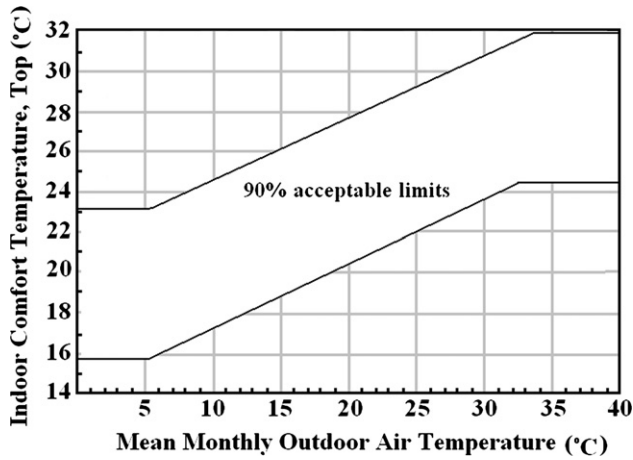


Fig. 2. Adaptive standard for naturally ventilated buildings.

2. Modeling the system

Modeling the system includes the models of two distinctive devices: the Solar Chimney (SC), and the Evaporative Cooling Cavity (ECC) shown in Figs. 3 and 4, respectively. For estimating the ventilation rate of the proposed solar house as a whole, it is important to determine the air flow rate which can be handled under a particular design and operating conditions. Therefore, an overall energy balance on the chimney is considered. This includes the energy balances for glass cover wall, the black absorber wall, and the air between. Writing the energy balance equations and solving them for T_g , T_{abs} , and T_f to calculate air flow rate have sought a mathematical solution. The chimney modeling has been done in accordance with Ong model [10]. Indoor thermal comfort condition depends on room air temperature. A simplified steady state model is developed to determine the air mean temperature

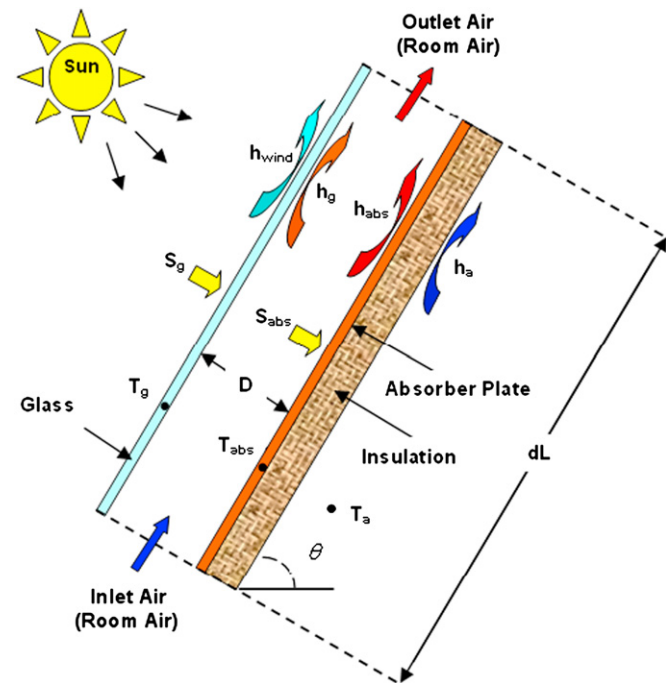


Fig. 3. Schematic diagram of the heat transfers in the solar chimney.

at the outlet of cooling cavity and room air temperature. For modeling the cooling cavity, heat and mass transfer from the water film into the air flow and the overall energy balance equations are taken into account.

Some postulations are assumed to enable solving the mathematical model. The major assumptions are summarized as follows:

1. The air at the room is at a uniform temperature.
2. Air enters the chimney at room air temperature.
3. Only buoyancy force is considered and wind induced natural ventilation is not included.
4. The flows in the channels are laminar, and hydrodynamically and thermally are fully developed.
5. The glass cover is opaque for infrared radiation.
6. Thermal capacities of glass and wall are negligible.
7. The air flow in the channel is radiative non-participating medium.
8. All thermophysical properties are evaluated at an average temperature.
9. Thermal resistance of water film is negligible.
10. The spray enthalpy is negligible.
11. The air enthalpy is only expressed as a linear function of wet bulb temperature.
12. The Lewis number relating heat and mass transfer is 1.0.
13. The system is at steady-state condition.

2.1. Mathematical modeling of solar chimney

An element of the modeled SC is shown in Fig. 3. Based on the energy conservation law, a set of differential equations are obtained along the length of the SC. The energy balance equation for the glass cover is:

$$S_g A_g + hr_{abs-g} A_{abs} (T_{abs} - T_g) = h_g A_g (T_g - T_{fsc}) + U_{g-a} A_g (T_g - T_{fsc}) \quad (1)$$

The overall top heat loss coefficient from the glass cover to ambient air (U_{g-a}), can be written as:

$$U_{g-a} = h_{wind} + hr_{g-sky} + h_{g-a} \quad (2)$$

The convective heat transfer coefficient due to the wind is given by Ref. [11] as follow:

$$h_{wind} = 2.8 + 3.0 u_{wind} \quad (3)$$

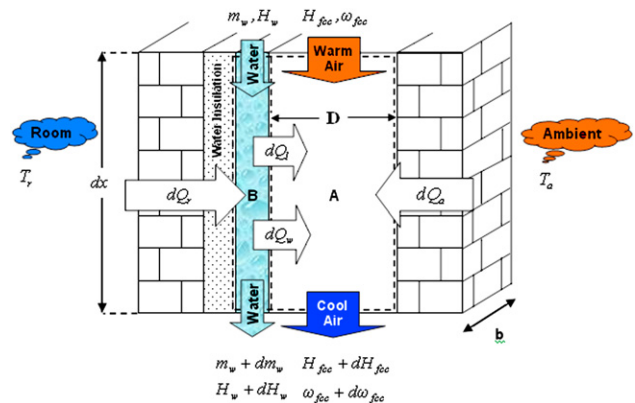


Fig. 4. Schematic diagram of heat and mass transfer in the cooling cavity.

The solar radiation heat flux absorbed by the glass cover is given by:

$$S_g = \alpha_g I \quad (4)$$

The radiative heat transfer coefficient from the outer glass surface to the sky considering the ambient temperature is adopted from Ref. [10]:

$$hr_{g\text{-sky}} = \frac{\sigma \varepsilon_g (T_g + T_{\text{sky}}) (T_g^2 + T_{\text{sky}}^2) (T_g - T_{\text{sky}})}{(T_g - T_a)} \quad (5)$$

where, the sky temperature is $T_{\text{sky}} = 0.0552 T_a^{1.5}$ [11].

The radiation heat transfer coefficient between the absorber plate and the glass cover is [10]:

$$hr_{\text{abs-g}} = \frac{\sigma (T_g^2 + T_{\text{abs}}^2) (T_g + T_{\text{abs}})}{(1/\varepsilon_g + 1/\varepsilon_{\text{abs}} - 1)} \quad (6)$$

The convective heat transfer coefficient between the glass cover and the air flow in the chimney:

$$h_g = \text{Nu}_g k_{\text{fsc}} / L_g \quad (7)$$

where, Nusselt number is given by $\text{Nu}_g = 0.6(\text{Gr}_g \cos\theta \text{Pr}_{\text{fsc}})^{0.2}$ and Grashof number is calculated from $\text{Gr}_g = (g\beta S_g (L_g)^4 / (k_{\text{fsc}} \nu_{\text{fsc}}^2))$ [12]. The convective heat transfer coefficient between the inclined absorber wall and the air flow in the chimney is given by:

$$h_{\text{abs}} = \text{Nu}_{\text{abs}} k_{\text{fsc}} / L_{\text{sc}} \quad (8)$$

All property values are evaluated at an average surface – air temperatures. The energy balance equation for the air flow in the chimney is:

$$h_{\text{abs}} A_{\text{abs}} (T_{\text{abs}} - T_{\text{fsc}}) + h_g A_g (T_g - T_{\text{fsc}}) = -m C_{\text{fsc}} (T_{\text{fsc}} - T_r) / \gamma \quad (9)$$

The axial mean air temperature has been experimentally determined to follow the non-linear form [10]:

$$T_{\text{fsc}} = \gamma T_{\text{fsc0}} + (1 - \gamma) T_{\text{fscin}} \quad (10)$$

where γ is a constant and recommended as 0.74. The energy balance equation for the absorber plate is written as:

$$S_{\text{abs}} A_{\text{abs}} = h_{\text{abs}} A_{\text{abs}} (T_{\text{abs}} - T_{\text{fsc}}) + hr_{\text{abs-g}} A_{\text{abs}} (T_{\text{abs}} - T_g) + U_{\text{abs-a}} A_{\text{abs}} (T_{\text{abs}} - T_a) \quad (11)$$

The overall heat transfer coefficient from the rear of the absorber wall to the ambient ($U_{\text{abs-a}}$) is given by:

$$U_{\text{abs-a}} = 1 / (1/h_a + \delta_{\text{ins}}/k_{\text{ins}}) \quad (12)$$

In the above equation h_a has been taken as 2.8 W/m² K [11].

2.2. Mathematical modeling of ECC

From the energy and mass conservation laws, a set of differential equations are considered along the length of the cooling cavity as shown in Fig. 4.

The convective heat transfer from the water film into the air flow is given by:

$$dQ_w = h_{\text{fcc}} f (T_w - T_{\text{fcc}}) dA \quad (13)$$

where, dA is equal to $b dx$, and f represents wettability percentage of the plate. h_{fcc} is defined as the dry heat transfer coefficient calculated using any relevant correlation for a flow between parallel plates [13]. The following relation is adopted in this study:

$$h_{\text{fcc}} = 57 (u_{\text{fcc}})^{0.7} \quad (14)$$

The heat transfer from the room air into the water film is obtained from:

$$dQ_r = U_{r-w} (T_r - T_w) dA \quad (15)$$

The heat transfer from the ambient into the air flow is obtained from:

$$dQ_a = U_{a-fcc} (T_a - T_{\text{fcc}}) dA \quad (16)$$

The overall heat transfer coefficients from the room to the water film and from ambient to the air flow are given by:

$$U_{r-w} = \frac{1}{\frac{1}{h_r} + \frac{1}{h_{\text{water}}} + \frac{\delta_{\text{wall}}}{k_{\text{wall}}} + \frac{\delta_{\text{ins}}}{k_{\text{ins}}}} \quad (17.a)$$

$$U_{a-fcc} = \frac{1}{\frac{1}{h_a} + \frac{\delta_{\text{wall}}}{k_{\text{wall}}} + \frac{1}{h_{\text{fcc}}}} \quad (17.b)$$

For steady, fully developed, two-dimensional flow of a laminar film along a vertical surface, the water side film heat transfer coefficient can be expressed as [14]:

$$h_w = \frac{k_w}{\delta_w} \quad (18.a)$$

where:

$$\delta_w = \left(\frac{3u_w^2}{4g} \right)^{1/3} (\text{Re}_w)^{1/3} \quad (18.b)$$

$$\text{Re}_w = \frac{m_w}{l\mu_w} \quad (18.c)$$

$$u_w = 1.5 \left(\frac{\nu_w g}{48} \right)^{1/3} (\text{Re}_w)^{2/3} \quad (18.d)$$

The heat transfer due to water evaporation (latent heat transfer) is given by:

$$dQ_l = dm_w H_{\text{pw}} \quad (19)$$

The specific enthalpy of water vapor is almost a linear function of temperature [15]:

$$H_{\text{pw}} = C_{\text{pv}} T_w + H_{\text{fg}} \quad (20)$$

The mass flow rate of water (dm_w) that is evaporated into the air flow is given by:

$$dm_w = h_{\text{mf}} (\omega_{\text{fcc}(T_w)} - \omega_{\text{fcc}}) dA \quad (21)$$

$$m_{\text{fcc}} d\omega_{\text{fcc}} = dm_w \quad (22)$$

The overall energy balance for the control volume of air, A , shown in Fig. 4 both for cocurrent and countercurrent flow configurations (Fig. 5) is given by:

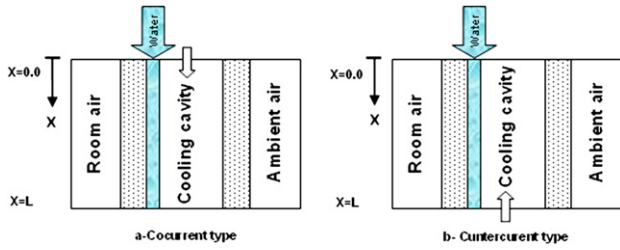


Fig. 5. Boundary conditions.

$$m_{fcc} (C_p T_{fcc} + \omega_{fcc} H_{fcc}) + dQ_w + dQ_l + dQ_a = m_{fcc} (C_p (T_{fcc} + dT_{fcc}) + (\omega_{fcc} + d\omega_{fcc}) (H_{fcc} + dH_{fcc})) \quad (23)$$

The energy balance equation for the control volume *B* shown in Fig. 4 is given by:

$$m_{fcc} dH_{fcc} + dQ_r = m_w dH_w + H_w dm_w \quad (24)$$

The enthalpy of humid air is equal to the sum of the enthalpies of the dry air and the water vapor, and it can be expressed as [15]:

$$H_f = C_p T_f + \omega_f (C_{pv} T_{fcc} + H_{fg}) \quad (25)$$

The enthalpy of water is given by Ref. [14]:

$$H_w = C_{pw} T_w \quad (26)$$

Inserting equations (13), (15), (16), (19) into equations (21)–(24) result in the following ordinary differential equations:

$$\frac{d\omega_{fcc}}{dx} = -\frac{h_m f b (\omega_{fcc(T_w)} - \omega_{fcc})}{m_{fcc}} \quad (27)$$

$$\frac{dT_{fcc}}{dx} = \frac{bh_{fcc}f(T_w - T_{fcc})}{m_{fcc}C_p} + \frac{H_{fcc(T_w)} - H_{fcc}}{C_p} \frac{d\omega_{fcc}}{dx} + \frac{bU_{a-fcc}(T_a - T_{fcc})}{m_{fcc}C_p} \quad (28)$$

$$\frac{dT_w}{dx} = \left[m_{fcc} \frac{dH_{fcc}}{dx} + b(U_{r-w}f(T_r - T_w) - m_{fcc}C_{pw}T_w \frac{d\omega_{fcc}}{dx}) \right] / m_w C_{pw} \quad (29)$$

The required boundary conditions for solving equations (21)–(24) in a cocurrent configuration are:

$$T_{fcc}(0.0) = T_a, T_w(L) = T_w(0.0) \quad (30.a)$$

$$RH_{fcc}(0.0) = RH_a \quad (30.b)$$

And for countercurrent flow are:

$$T_{fcc}(L) = T_a, T_w(L) = T_w(0.0) \quad (31.a)$$

$$RH_{fcc}(L) = RH_a \quad (31.b)$$

In an actual application of the system, one might face some limitations in using cocurrent and countercurrent configurations. In this case, cross flow configuration may be used. This case is very similar to the previous configurations, but the air flow direction is perpendicular to that of water flow. An infinitesimal element for

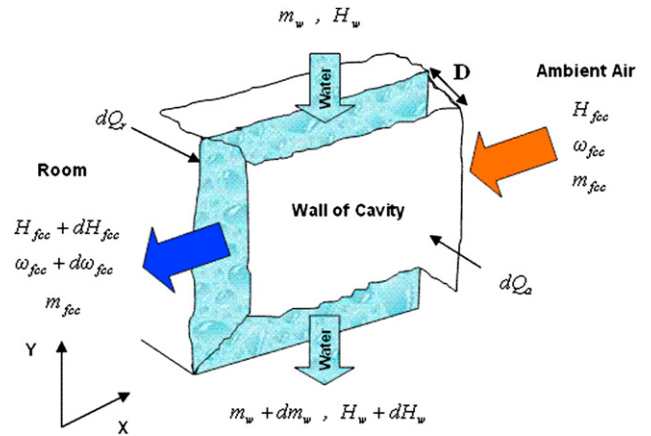


Fig. 6. Schematic diagram of the heat and mass transfer in cross flow cooling cavity.

modeling of this type is shown in Fig. 6. A set of differential equations by expanding energy balance equations are obtained as follows:

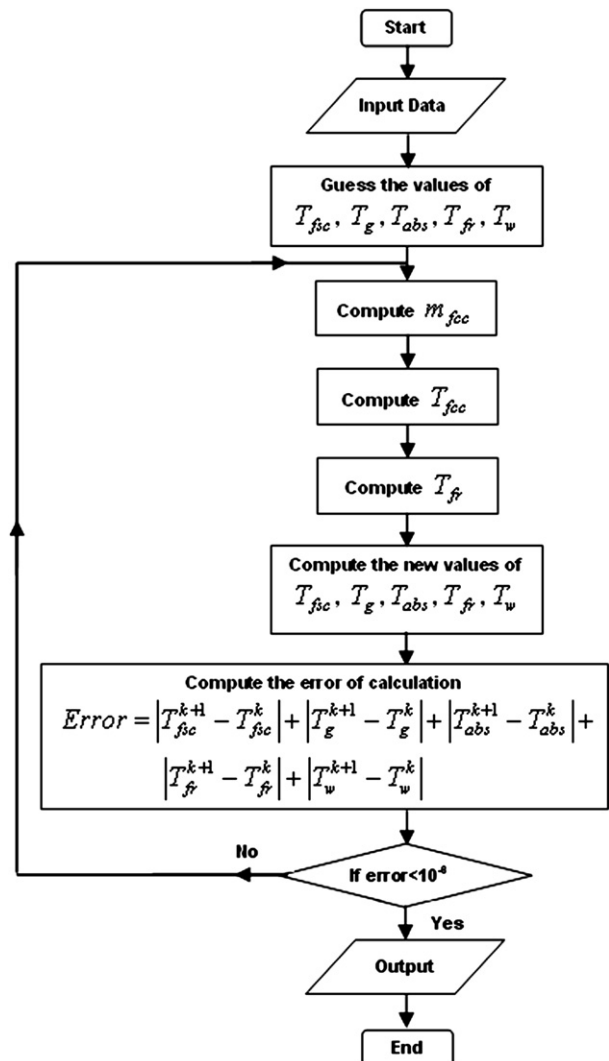


Fig. 7. Flow chart of the solving procedure.

Table 1
Thermophysical properties.

Parameters	Value
1. Transmissivity of glass	0.84
2. Absorptivity of glass	0.06
3. Emissivity of the glass	0.90
4. Absorptivity of absorber wall	0.95
5. Emissivity of the absorber surface	0.95
6. Thermal conductivity of the break wall	0.72 (Wm ⁻¹ K ⁻¹)
7. Thickness of break wall	0.10 (m)
8. Thermal conductivity of SC and ECC insulation	0.16 (Wm ⁻¹ K ⁻¹)
9. Thickness of SC and ECC insulation	0.002 (m)

$$\frac{dT_{fcc}}{dx} = \frac{H_{fcc}(T_w) - H_{fcc}}{C_p} \frac{d\omega_{fcc}}{dx} + \frac{h_{fcc}f(T_w - T_{fcc})}{m_{fcc}C_p} dy + \frac{U_{a-fcc}(T_a - T_{fcc})}{m_{fcc}C_p} dy \quad (32)$$

$$\frac{dT_w}{dy} = \left(U_{r-w}f(T_r - T_w)dx + m_{fcc}C_p \frac{dT_{fcc}}{dy} - m_{fcc}C_{pw}T_w \frac{d\omega_{fcc}}{dy} \right) / m_w C_{pw} \quad (33)$$

$$\frac{d\omega_{fcc}}{dx} = - \frac{h_{mf}(\omega_{fcc}(T_w) - \omega_{fcc})}{m_{fcc}} dy \quad (34)$$

Differential equations (32)–(34) describe the operation of a cross flow cooling cavity. Boundary conditions for cross flow configuration are:

$$T_{fcc}(L, y) = T_a, T_w(x, 0.0) = T_w(x, L) \quad (35.a)$$

$$RH_{fcc}(L, y) = RH_a \quad (35.b)$$

There are three equations including four unknown variables (ω_{fcc} , T_{fcc} , T_w and T_r) which describe the process of heat and mass transfer in ECC. An iterative procedure is used to solve the set of equations. The water film temperature is estimated and other parameters are determined. Then the determined value of T_w is compared to the estimated one, and the procedure is iterated until convergence is achieved.

2.3. Ventilation

Chimney effect is the buoyancy driven movement of air into and out of the buildings. Buoyancy occurs due to the difference between indoor and outdoor air density resulting from temperature and

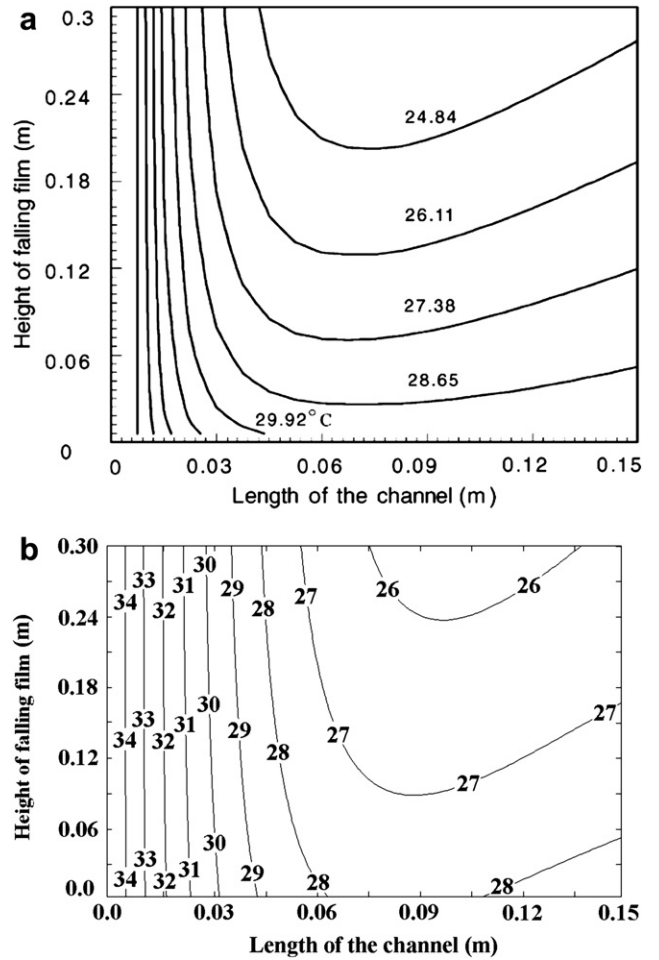


Fig. 8. a. Result of Ref. [19], b. Result of the present study.

moisture differences. A chimney heated by solar energy can be used to induce the stack effect without increasing the room temperature. The driving potential for the air flow through the solar house is a function of the pressure difference between the cooling cavity inlet and the SC outlet. The buoyancy pressure due to the increasing air temperature in the SC sucks the cooled heavy air through the cooling cavity. The friction losses due to fluid flow through the channels and across the fittings refrain from the fluid flow. If the buoyancy pressure overcomes the sum of all flow pressure losses, the natural ventilation will take place.

A mathematical model based on *Bernoulli's* equation is used to estimate the system flow rate. The chimney net draft can be calculated by the following formula [16]:

Table 2
Comparison of experimental and theoretical results for solar chimney included ACH No.

Solar radiation (W/m ²)	Absorber length (m)	Inlet chim. dimens. (m × m)	Ambient temp. (K)	ACH			Errors of [18] (%)	Errors of present study (%)
				EXP [18].	Theo. [18].	Theo. (present study)		
300	0.7	1.0 × 0.3	295–302	4.400	4.173	3.994	5.16	9.23
	0.8	1.0 × 0.2	298–304	5.330	4.054	3.657	23.94	31.39
	0.9	1.0 × 0.1	294–296	2.400	2.704	2.803	12.66	16.79
500	0.7	1.0 × 0.3	295–302	4.800	5.160	4.900	7.50	2.08
	0.8	1.0 × 0.2	298–304	4.530	4.895	4.679	8.06	3.29
	0.9	1.0 × 0.1	294–296	2.660	3.461	3.442	30.11	29.40
700	0.7	1.0 × 0.3	295–302	5.600	5.810	5.800	3.75	3.57
	0.8	1.0 × 0.2	298–304	5.330	5.175	5.315	2.91	0.28
	0.9	1.0 × 0.1	294–296	2.930	3.671	3.319	25.29	13.27

$$\text{Draft}_{sc} = (\rho_{fa} - \rho_{fsc})gL_{sc}\sin\theta - \left(\sum_{j=3}^5 c_j + \xi_{sc} \frac{L_{sc}}{(d_{hyd})_{sc}} \right) \times \left(\frac{\rho_{fsc}u_{sc}^2}{2} \right) \quad (36)$$

where, c_j is the pressure loss coefficients at the locations which are indicated in Fig. 1.

In equation (36), the first term is the chimney theoretical draft and the second one is the chimney pressure loss. The cooling cavity pressure loss is [17]:

$$\Delta P_{cc} = \left(\sum_{j=1}^2 c_j + \xi_{cc} \frac{L_{cc}}{(d_{hyd})_{cc}} \right) \left(\frac{\rho_{fcc}u_{fcc}^2}{2} \right) \quad (37)$$

where:

$$\xi = \frac{64}{Re} \quad \text{if } Re < 2300 \quad (38.a)$$

$$\xi = (1.82 \log Re - 1.64)^{-2} \quad \text{if } Re \geq 2300 \quad (38.b)$$

The air temperature at the solar chimney inlet is assumed to be same as the room air temperature; however, it may differ from the air temperature at the cooling cavity outlet due to occupant's heat generation. Therefore, the stack effect in the cooling cavity and the room can be expressed as:

$$\text{Draft}_{cc} = (\rho_{fcc} - \rho_{fa})gL_{cc} \quad (39)$$

$$\text{Draft}_r = (\rho_{fr} - \rho_{fcc})gL_r \quad (40)$$

The required draft for the cooling system (Draft_{ccr}) is the sum of the cavity pressure loss and the negative pressures Draft_{cc} and Draft_r .

$$\text{Draft}_{ccr} = \Delta P_{cc} - \text{Draft}_{cc} - \text{Draft}_r \quad (41)$$

The flow reaches a steady state when the chimney draft equals to the cooling system pressure drop.

$$\text{Draft}_{ccr} = \text{Draft}_{sc} \quad (42)$$

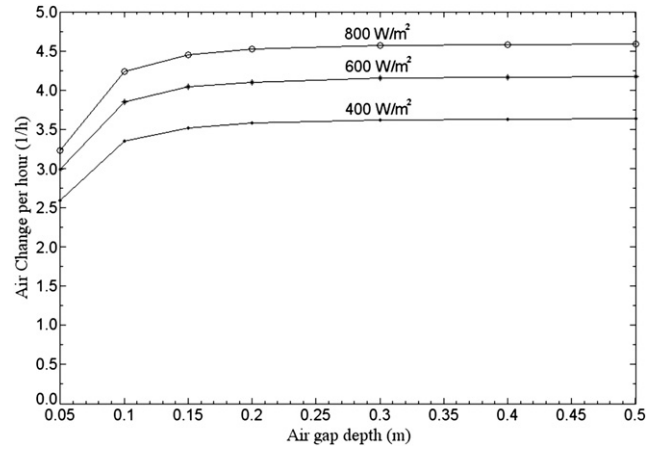


Fig. 9. The effect of the air gap depth on the ACH.

The air flow mass at the chimney and the ECC are equal if there is no air infiltration:

$$m = \rho Au| = \rho Au|_{ECC} \quad (43)$$

Using equations (42) and (43), the air velocity in the SC can be obtained as:

$$u_{fsc} = \sqrt{\frac{\text{Buoyancy Terms}}{\text{Friction Terms}}} \quad (44.a)$$

where:

$$\text{Buoyancy Terms} = 2 \left\{ (\rho_{fa} - \rho_{fsc})gL_{sc}\sin(\theta) - (\rho_{fcc} - \rho_{fr})gL_r + (\rho_{fcc} - \rho_{fa})gL_{cc} \right\} \quad (44.b)$$

$$\begin{aligned} \text{Friction Terms} = & \left\{ c_5 + \xi_{sc} \frac{L_{sc}}{(d_{hyd})_{sc}} \right\} \rho_{fsc} + c_4 \left(\frac{\rho_{fsc}A_{sco}}{\rho_r A_{sco}} \right)^2 \rho_{fr} \\ & + c_3 \left(\frac{\rho_{fsc}A_{sco}}{\rho_r A_{scin}} \right)^2 \rho_{fr} + c_2 \left(\frac{\rho_{fsc}A_{sco}}{\rho_{fcc}A_{cc}} \right)^2 \rho_{fcc} \\ & + c_1 \left(\frac{\rho_{fsc}A_{sco}}{\rho_{fa}A_{cc}} \right)^2 \rho_{fa} \\ & + \xi_{cc} \frac{L_{cc}}{(d_{hyd})_{cc}} \left(\frac{\rho_{fsc}A_{sco}}{\rho_{fcc}A_{cc}} \right)^2 \rho_{fcc} \end{aligned} \quad (44.c)$$

Table 3
Theoretical results for different solar radiation.

Type of ECC of	Solar radiation (W/m ²)	Inlet chimney dimensions ($W_{in} \times Z$) (m × m)	ACH	Air temperature at the outlet of ECC (°C)	Room air temperature (°C)	Room air relative humidity (%)	Number SC
Cocurrent	200	0.4 × 0.1	2.85	25.26	27.76	73.75	1
	400		3.58	25.49	27.48	71.97	1
	600		4.10	25.64	27.38	71.35	1
	800		4.52	25.75	27.33	70.16	1
	1000		4.87	25.84	27.31	69.58	1
Contercurrent	200	0.4 × 0.1	–	–	–	–	–
	400		2.60	28.22	30.87	75.06	1
	600		3.24	28.31	30.53	73.33	1
	800		3.74	28.45	30.37	72.21	1
	1000		4.15	28.58	30.28	71.40	1
Crossflow	200	0.4 × 0.1	2.23	28.83	32.08	68.45	1
	400		3.06	28.22	29.02	66.23	1
	600		3.65	29.12	31.10	65.45	1
	800		4.12	29.20	30.95	64.71	1
	1000		4.50	29.25	30.85	64.16	1

Table 4

Theoretical results for different solar absorber length.

Ambient temperature (°C)	Solar radiation (W/m ²)	Absorber length (m)	Inlet chimney dimensions ($W_{in} \times Z$) (m × m)	ACH —	Room air temperature (°C)	Number of SC
34	200	2.0	0.4 × 0.1	2.66	27.88	1.0
	400			2.98	27.70	1.0
	600			3.24	27.59	1.0
	800			3.45	27.52	1.0
	1000			3.64	27.47	1.0
34	200	3.0	0.4 × 0.1	2.72	27.84	1.0
	400			3.26	27.58	1.0
	600			3.66	27.46	1.0
	800			3.98	27.40	1.0
	1000			4.26	27.36	1.0
34	200	4.0	0.4 × 0.1	2.85	27.76	1.0
	400			3.58	27.48	1.0
	600			4.10	27.38	1.0
	800			4.52	27.33	1.0
	1000			4.87	27.31	1.0
34	200	5.0	0.4 × 0.1	3.02	27.67	1.0
	400			3.91	27.41	1.0
	600			4.54	27.33	1.0
	800			5.04	27.30	1.0
	1000			5.46	27.29	1.0
34	200	6.0	0.4 × 0.1	3.20	27.60	1.0
	400			4.25	27.36	1.0
	600			4.98	27.30	1.0
	800			5.55	27.29	1.0
	1000			6.03	27.29	1.0

The air change number per hour is calculated under steady-state conditions and is given by the following relation [12]:

$$ACH = \frac{3600 m}{\rho_{fcc} V_r} \quad (45)$$

3. Numerical solution

The coupled governing equations (1), (9), (11) and (27)–(29) or (30)–(32) are the full description of the system. A computer

program is written in MATLAB software for solving the set of equations. The governing equations have to be solved iteratively until convergence of the results. Here, the finite difference method is used for solving the ECC equations in accordance with the procedures which is shown in Fig. 7. A finer mesh size has been used to give an acceptable accuracy and a careful examination on grid-independence of the numerical solutions has been made to ensure the accuracy and validity of the numerical results. Through the calculation, the properties of air, water and air–water vapor mixture are assumed constant at each step of the numerical calculation. Formulas used to calculate the fluid physical properties

Table 5

Theoretical results for different inlet chimney dimensions.

Ambient temperature (°C)	Solar radiation (W/m ²)	Absorber length (m)	Inlet chimney dimensions ($W_{in} \times Z$) (m × m)	ACH —	Room air temperature (°C)	Number of SC
34	200	4.0	0.1 × 0.1	–	–	–
			0.2 × 0.1	1.80	28.89	1.0
			0.4 × 0.1	2.85	27.76	1.0
			0.6 × 0.1	3.58	27.48	1.0
			0.8 × 0.1	4.07	27.38	1.0
			1.0 × 0.1	4.42	27.34	1.0
			1.2 × 0.1	4.66	27.32	1.0
34	600	4.0	0.1 × 0.1	1.57	29.40	1.0
			0.2 × 0.1	2.60	27.92	1.0
			0.4 × 0.1	4.10	27.38	1.0
			0.6 × 0.1	5.13	27.30	1.0
			0.8 × 0.1	5.85	27.29	1.0
			1.0 × 0.1	6.34	27.30	1.0
			1.2 × 0.1	6.70	27.30	1.0
34	1000	4.0	0.1 × 0.1	1.87	28.76	1.0
			0.2 × 0.1	3.09	27.64	1.0
			0.4 × 0.1	4.87	27.31	1.0
			0.6 × 0.1	6.09	27.29	1.0
			0.8 × 0.1	6.94	27.32	1.0
			1.0 × 0.1	7.53	27.34	1.0
			1.2 × 0.1	7.95	27.36	1.0

at an average surface – air temperatures are given by empiric correlations (46)–(49) fitted for the 300–350 K interval [10].

$$\mu_f = (1.846 + 0.00472(T_f - 300)) \times 10^{-5} \quad (46)$$

$$\rho_f = 1.164 - 0.00353(T_f - 300) \quad (47)$$

$$k_f = 0.0263 + 0.000074(T_f - 300) \quad (48)$$

$$C_f = (1.007 + 0.00004(T_f - 300)) \times 10^3 \quad (49)$$

4. Analysis

The capability of the system to provide the desired indoor conditions depends on several parameters such as the ambient conditions (temperature, solar radiation), dimensions of SC, ECC and room specifications. Parametric study is carried out to find the effects of geometrical dimensions of the SC, ECC on the system performance under various outdoor environmental conditions.

The following dimensions and specifications are applied in the modeling: The system is located in Tehran, having 35.44°N latitude position, a south facing solar chimney with the length of 4.0 m and air gap depth of 0.2 m is considered. A detailed study on solar chimney found the optimum angle of 50° to capture more radiation [12]. The ECC is a Cubic channel with the height of 2.0 m and 2.0 m × 0.1 m inside cross section. The wettability percent of wetted wall is 0.7.

The calculations are carried out for a room, having a size of 4.0 m × 4.0 m × 3.125 m without air infiltration. The cooling air emerges from the ECC outlet and enters the SC inlet which is located on the opposite wall. The ECC outlet is lowered 2.0 m below the SC inlet (Fig. 1). The cooling load is considered to be 116 W, which is equal to the heat generated by one person at rest. The indoor room air temperature is kept in the thermal comfort range (Fig. 2) to secure the desired condition inside the room space. The ambient air temperature, relative humidity and wind velocity are 34 °C, 30% and 1.0 m/s, respectively. The thermophysical properties of the materials included in the modeling are given in Table 1. The values of the properties specified in the table are kept constant in the computation unless specifically noted otherwise. In order to check the mathematical model and to evaluate the accuracy of the present results, the calculation has been carried out for same conditions of experimental and theoretical results of Refs. [18] and [19], respectively. Ref. [18] has reported the experimental results of the SC performance based on ACH number for various solar radiations and geometrical dimensions. The quantitative comparison shows a reasonable agreement between the results obtained by the present theoretical study and the published results of Ref. [18] as given in Table 2. The theoretical results of this study are in good coincidence with theoretical results of Ref. [18]. However, there is a considerable difference between the theoretical results and experimental results which amounts to about 30%. This difference is due to the wind effect on the experimental results (as reported by Ref. [18]) which is being neglected in the theoretical results.

Fig. 8 shows the patterns of temperature contours of air and indicates that the calculated values of the present model agree reasonably well with the theoretical results of Ref. [19]. The small difference is due to the thermal resistance of the heat exchanger's wall which has been considered in the present model but neglected in Ref. [19]. Therefore, it is reasonable to conclude that the obtained temperatures of the present study are slightly higher than of Ref. [19]. However, the present mathematical model can predict the

air flow rate and air temperature quite accurately and the calculated results are reliable.

5. Results and discussion

5.1. System performance

Theoretical calculations are performed for various solar radiation intensities and the results are summarized in Table 3. According to the adaptive comfort standard, the acceptable mean air temperatures are in the range of 27.31–31.10 °C and therefore the calculated indoor air temperatures at various solar radiations are within the acceptable range. In all cases, the ventilation rate was found to be approximately around 3 air changes per hour even at the poor solar radiation of 200 W/m². Passive ventilation standards require a minimum of 3 air changes for residential buildings [20]. Therefore, it can be concluded that the proposed system is able to provide the desired ventilation and thermal needs of inhabitants even in low solar radiation.

The results show that the air and flow configuration through the ECC influence the performance of the system. The performance of the systems with different flow type can be assessed on the Saturation Efficiency (SE), defined as:

$$SE = \frac{T_{db,a} - T_{db,cco}}{T_{db,a} - T_{wb,a}} \quad (50)$$

Comparison of the calculated results of the saturation efficiency for different configurations results in:

$$SE_{Cocurrent} > SE_{Countercurrent} > SE_{Crossflow} \quad (51)$$

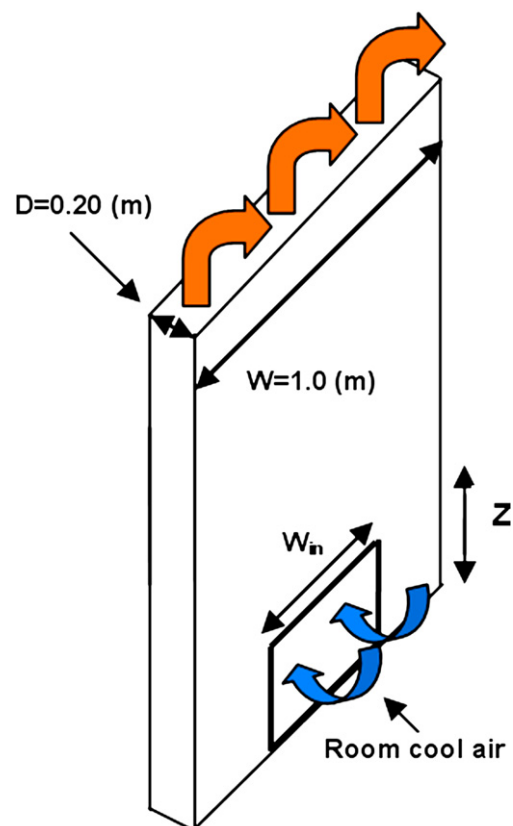


Fig. 10. Schematic diagram of the chimney.

Thus, the design of the system with cocurrent configuration leads to higher performance and it is recommended accordingly.

5.2. Effects of the system dimensions and wettability factor on performance

The effects of SC and ECC dimensions on the system performance are investigated in the following sections. The same values of the parameters specified in the previous sections are used in the computation and the flow configuration through ECC is cocurrent unless specifically noted hereby.

5.2.1. Effects of SC dimensions

Fig. 9 shows a plot of air change for the room at different air gap depths and different solar radiation values. It shows that the effect of air gap depth on the ACH is significant up to 0.2 m and beyond 0.2 m, the ACH remains almost constant. An Air gap of 0.2 m is considered as the maximum required value of the air gap. The results showed that a better performance would be achieved at a higher solar radiation heat flux. This means that around the noon, when the cooling effect is most needed, the system reaches its highest effectiveness.

The results also show that the ACH is increased by adding the absorber wall length (Table 4). This is due to enhancement of the stack effect of the SC with the increase of L_{SC} as given by Eq. (36).

Another parameter that affects the system performance is the chimney inlet dimensions. The results given in Table 5, show the

desired room air temperature and ACH could be achieved by several different combinations of inlet dimensions. By increase of chimney inlet width (W_{in}) (Fig. 10), the chimney inlet area increases and according to equation (44.c), the friction force decreases and causes an increase in ACH. The result shows, when the solar radiation is low, the room air temperature and ACH number would stay in the permitted range of the thermal comfort if the size of chimney inlet has been regulated correctly. A design of SC with variable inlet may assist the inhabitants to set the inside room temperature together with the ACH number to the favorite values.

5.2.2. Effects of ECC dimensions

Table 6 shows the effect of ECC dimensions on the system performance and indoor conditions under various ambient air temperatures and solar radiations. It is found that a lower room air temperature can be achieved with a higher cavity length because of the increase of evaporation area which leads to more heat and mass transfers. Comparison between the results shows that the design of ECC with the height of 2.0 m may be suitable for the present configuration; however, it is necessary to increase the cavity width if the ambient air temperature is higher than 34 °C.

Another important parameter which affects the system performance is the air gap depth of ECC. Table 6 shows a small gap depth results in high pressure drop in the channel. However, it causes low ACH and low air velocity in ECC, and high evaporation rate which leads to lower air temperature at ECC outlet. Thus, the decrease of the cavity depth has two different effects. Therefore it is necessary

Table 6
Theoretical results for different ECC height.

Ambient temperature (°C)	Solar radiation (W/m ²)	Inlet chimney dimensions ($W_{in} \times Z$) (m × m)	ECC dimensions ($W_{ECC} \times L_{ECC}$) (m × m)	ECC depth (m)	ACH —	Room air temperature (°C)	Number of SC		
34	200	0.4 × 0.1	2.0 × 1.0	0.05	2.13	26.48	1.0		
				0.10	2.40	28.81	1.0		
				0.15	2.47	30.22	1.0		
		2.0 × 1.5	0.05	2.35	25.88	1.0			
			0.10	2.62	28.19	1.0			
			0.15	2.67	29.66	1.0			
			2.0 × 2.0	0.05	2.55	25.49	1.0		
				0.10	2.86	27.76	1.0		
				0.15	2.88	29.26	1.0		
34	1000	0.4 × 0.1	2.0 × 1.0	0.05	4.13	25.67	1.0		
				0.10	4.65	28.21	1.0		
				0.15	4.78	29.58	1.0		
			2.0 × 1.5	0.05	4.21	25.13	1.0		
				0.10	4.75	27.67	1.0		
				0.15	4.87	29.10	1.0		
		2.0 × 2.0	0.05	4.30	24.80	1.0			
			0.10	4.87	27.31	1.0			
			0.15	4.97	28.76	1.0			
		42	200	0.4 × 0.1	2.0 × 1.0	0.05	2.18	33.49	1.0
						0.10	2.45	35.98	1.0
						0.15	2.52	37.46	1.0
2.0 × 1.5	0.05				2.42	32.68	1.0		
	0.10				2.70	35.16	1.0		
	0.15				2.74	36.69	1.0		
2.0 × 2.0	0.05			2.65	32.11	1.0			
	0.10			2.96	34.57	1.0			
	0.15			2.98	36.12	1.0			
42	1000			0.4 × 0.1	2.0 × 1.0	0.05	4.16	32.97	1.0
						0.10	4.68	35.64	1.0
						0.15	4.81	37.08	1.0
		2.0 × 1.5	0.05		4.25	32.30	1.0		
			0.10		4.79	34.97	1.0		
			0.15		4.91	36.46	1.0		
		2.0 × 2.0	0.05	4.35	31.83	1.0			
			0.10	4.92	34.49	1.0			
			0.15	5.02	36.00	1.0			

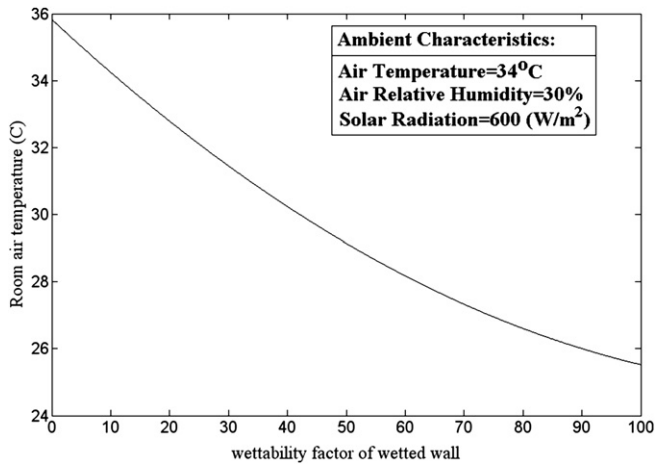


Fig. 11. The effect of ECC wettability on the room temperature.

to specify the optimum cavity depth. Accordingly, the program has been performed for the various cavity depths in the range of 0.0–15.0 cm. The results showed the design of ECC with the depth of 5.0 cm would lead to the best performance.

5.2.3. Effects of wettability factor

Fig. 11 shows that the room air temperature can be much reduced by increase of the wettability percentage of the plate. The air-moisture exchange surface will be increased by increase of the wettability percentage and the best results are obtained for 100

percent wettability. The increase of wetted surface enhances the evaporation process, decreases the air temperature and increases the humidity ratio.

5.3. Effects of environmental conditions on the system performance

The influences of solar radiation, ambient air temperature and humidity on ACH and room air temperature are investigated here. The ACH is affected by the “chimney effect” which depends on the density differences between ambient air and SC outlet air. This difference is increased when the solar radiation rises and therefore leads to higher ACH as shown in Table 7.

Comparison of the results of 34 °C and 50 °C show that the variation of ACH due to the variation of ambient temperature is not significant. However, the applicability of system to provide thermal comfort conditions is reduced at higher ambient air temperature.

The results show that at low ambient air temperatures, good indoor condition can be achieved in a wide range of the ambient air humidity. The results of Table 7 show, when ambient R.H. and temperature are less or equal to 50% and 40 °C, respectively, room air temperature and ACH would remain in the desired range of thermal comfort. It means that when air temperature rises, thermal comfort can be achieved in lower humidity. However, the use of the system at temperatures higher than 40 °C, does not provide good indoor conditions.

The results show that the proposed system can provide thermal comfort conditions even during the night with zero solar radiation (Table 8). It is due to the buoyancy effect in the cooling cavity which can draw the cooled air into the room. The buoyancy terms are

Table 7

Theoretical results for different solar radiation and ambient temperature (cocurrent type).

Ambient air temperature(°C)	Solar radiation (W/m ²)	Ambient air relative humidity (%)	ACH	Room air temperature (°C)	Room air relative humidity (%)	Number of SC
34	200	30	2.55	25.49	86.65	1
		40	2.51	27.00	88.82	1
		50	2.46	28.49	90.91	1
		60	2.42	29.97	92.90	1
		70	–	–	–	–
34	1000	30	4.30	24.80	82.91	1
		40	4.28	26.26	85.57	1
		50	4.27	27.71	88.15	1
		60	4.25	29.16	90.66	1
		70	4.23	30.61	93.10	1
37	200	30	2.59	27.98	86.76	1
		40	2.54	29.48	88.92	1
		50	2.50	30.97	91.00	1
		60	2.45	32.46	92.97	1
		70	–	–	–	–
37	1000	30	4.32	27.44	83.13	1
		40	4.30	28.91	85.75	1
		50	4.28	30.38	88.30	1
		60	4.27	31.84	90.78	1
		70	4.25	33.31	93.19	1
40	200	30	2.62	30.45	86.88	1
		40	2.58	31.96	89.02	1
		50	2.53	33.46	91.07	1
		60	2.49	34.95	93.03	1
		70	–	–	–	–
40	1000	30	4.33	30.07	83.34	1
		40	4.32	31.56	85.94	1
		50	4.30	33.04	88.46	1
		60	4.28	34.52	90.91	1
		70	4.26	36.00	93.29	1
50	200	30	2.75	38.71	87.24	1
50	1000	30	4.04	38.82	84.04	1

Note: the dimensions of ECC are taken as 2.0 m × 2.0 m × 0.05 m.

Table 8
Performance of the system at low solar radiation (cocurrent type).

Ambient air temperature (°C)	Solar radiation (W/m ²)	Ambient air relative humidity (%)	ACH	Room air temperature (°C)	Room air relative humidity (%)	Number of SC
34	0	30	1.85	26.43	88.80	1
	100		2.54	25.80	87.50	1
	200		2.55	25.49	86.65	1
40	0	30	1.97	31.01	88.76	1
	100		2.32	30.65	87.68	1
	200		2.62	30.45	86.88	1

Note: the dimensions of ECC are taken as 2.0 m × 2.0 m × 0.05 m.

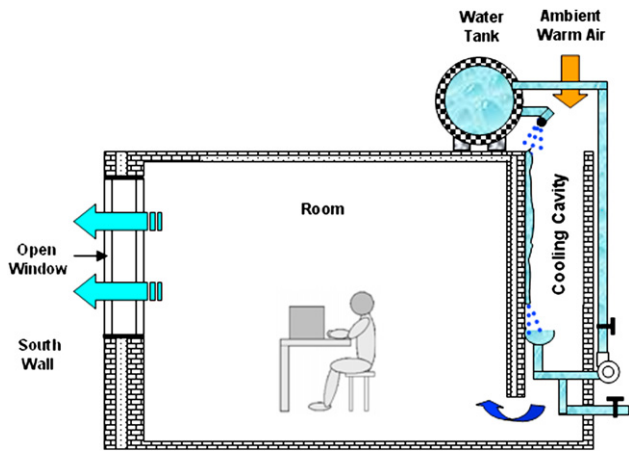


Fig. 12. Schematic diagram of the recommended system at night.

described by equation (44.b). At night, the first term which is the chimney effect is vanished and the second term has no significant effects. Therefore, the buoyancy effect of the ECC will be the dominant term. Anyhow, to reduce the pressure losses of the air flow during the night, the discharged air may leave the room through an opened window as shown in Fig. 12.

6. Conclusions

In this paper a new solar system employing a solar chimney together with an evaporative cooling cavity is proposed and studied. The numerical experiments show that this integrated system with proper configuration is capable of providing good indoor conditions at the daytime in a living room even at a poor solar intensity of 200 W/m² and high ambient air temperature of 40 °C. Although the performance strongly depends on the ambient air humidity; it is easy to prepare good indoor thermal conditions for ambient air relative humidity lower than 50% even at high ambient temperatures. As such, this technique is suitable to supply the cooling load in the moderate and arid climates.

The ventilation rate is influenced by solar radiation, ambient temperature, as well as geometrical configurations of both the SC and the ECC. The numerical experiments also show that the use of SC with variable inlet dimensions is a way to control the ACH and the air temperature of a room.

A combination of the proposed system with a conventional air-conditioning system would help to create a reasonable indoor environment for human thermal comfort as well as to be energy-efficient and environmentally friendly.

References

- [1] Bahadori MN. An improved design of wind towers for natural ventilation and passive cooling. *Solar Energy* 1985;35(2):119–25.

- [2] Verma R, Bansal NK, Garg HP. The comparative performance of different approaches to passive cooling. *Building and Environment* 1986;21(2):65–9.
- [3] Giabaklou Z, Ballinger JA. A passive evaporative cooling system by natural ventilation. *Building and Environment* 1996;31(6):503–7.
- [4] Aboulnaga M. A roof solar chimney assisted by cooling cavity for natural ventilation in buildings in hot arid climates: an energy conservation approach in AL-AIN city. *Renewable Energy* 1998;14(1–4):357–63.
- [5] Raman P, Mande S, Kishore VVN. A passive solar system for thermal comfort conditioning of buildings in composite climates. *Solar Energy* 2001;70(4):319–29.
- [6] Manzan M, Saro O. Numerical analysis of heat and mass transfer in passive building component cooled by water evaporation. *Energy and Buildings* 2002;34:369–75.
- [7] Dai YJ, Sumathy K, Wang RZ, Li YG. Enhancement of natural ventilation in a solar house with a solar chimney and adsorption cooling cavity. *Solar Energy* 2003;74:65–75.
- [8] Chungloo S, Limmeechokchai B. Application of passive cooling system in the hot and humid climate: the case study of solar chimney and wetted roof in Thailand. *Building and Environment* 2007;42:3341–51.
- [9] Brager GS, de Dear RJ. A standard for natural ventilation. *ASHRAE Journal* 2000;42(10):21–8.
- [10] Ong KS. A mathematical model of a solar chimney. *Renewable Energy* 2003;28:1047–60.
- [11] Duffie JA, Beckmann WA. *Solar engineering of thermal processes*. New York: Wiley Interscience, ISBN 0-471-05066-0; 1980.
- [12] Mathur J, Mathur S, Anupma. Summer-performance of inclined roof solar chimney for natural ventilation. *Energy and Buildings* 2006;38:1156–63.
- [13] Guo XC, Zhao TS. A parametric study of an indirect evaporative air cooler. *Heat and Mass Transfer* 1998;25(2):217–26.
- [14] Erens PJ, Dreyer AA. Modeling of indirect evaporative coolers. *International Journal of Heat and Mass Transfer* 1993;36(1):17–26.
- [15] Kloppers JC, Kroger DJ. A critical investigation into the heat and mass transfer analysis of counterflow wet-cooling towers. *International Journal of Heat and Mass Transfer* 2005;48:765–77.
- [16] ASHRAE handbook. HVAC systems and equipment, chimney, gas vent, and fireplace systems. p. 30.1–30.11. Atlanta, GA: American Society of Heating, Refrigerating and Airconditioning Engineers, Inc.; 2000.
- [17] ASHRAE handbook. Fundamentals, duct design. p. 34.1–34.6. Atlanta, GA: American Society of Heating, Refrigerating and Airconditioning Engineers, Inc.; 2000.
- [18] Mathur J, Bansal NK, Mathur S, Jain M, Anupma. Experimental investigations on solar chimney for room ventilation. *Solar Energy* 2006;80:927–35.
- [19] Dai YJ, Sumathy Jain K, Anupma. Theoretical study on a cross-flow direct evaporative cooler using honeycomb paper as packing material. *Applied Thermal Engineering* 2002;22:1417–30.
- [20] BIS, Bureau of Indian Standards. *Handbook of functional requirements of buildings*; ISBN 81-7061-011-7; 1997.

Nomenclature

- A: area (m²)
 ACH: air change per hour (h⁻¹)
 b: width of cooling cavity (m)
 C: specific heat of air (J/kg K)
 c: pressure loss coefficient of fittings (–)
 D: gap depth (m)
 d: diameter (m)
 f: wettability percent (%)
 H: enthalpy (KJ/kg)
 h_c: convective heat transfer coefficient (W/m² K)
 h_m: mass transfer coefficient (h_c/(Le.C)) (kg/s m²)
 hr: radiative heat transfer coefficient (W/m² K)
 I: incident solar radiation (W/m²)
 k: thermal conductivity (W/m K)
 L: length (m)
 m: mass flow rate of air (kg/s)
 Q: heat transfer to air stream (W/m²)
 RH: relative humidity (%)
 S: solar radiation heat flux absorbed by plate (W/m²)

SE: saturation efficiency

T: temperature (K)

U: overall heat transfer coefficient ($\text{W}/\text{m}^2 \text{K}$)

u: air velocity (m/s)

V: volume (m^3)

W: width (m)

x, y: coordinate system (m)

Z: height of chimney inlet (m)

Greek symbols

α : absorption coefficient (–)

β : volumetric coefficient of expansion (K^{-1})

γ : constant for mean temperature approximation (–)

ϵ : emissivity (–)

θ : angle (–)

μ : laminar viscosity ($\text{Kg}/\text{s m}$)

ν : kinematic viscosity ($\text{m}^2 \text{s}^{-1}$)

ξ : friction factor (–)

ρ : density (Kg/m^3)

σ : Stefan–Boltzmann constant ($5.67 \times 10^{-8} \text{W}/\text{m}^2 \text{K}^4$)

ω : humidity ratio ($(\text{Kg})_{\text{water}}/(\text{Kg})_{\text{air}}$)

Dimensionless terms

Gr: Grashof number [$g\beta_f(T - T_f)L^3/\nu^2$]

Nu: Nusselt number [$h_f L/\mu_f$]

Pr: Prandtl number [$C_f \mu_f/k_f$]

Re: Reynolds number [$u_f D_{\text{hyd}}/\nu_f$]

Subscripts

a: ambient

abs: absorber wall

cc: cooling cavity

db: dry bulb

f: air flow

fg: latent heat

g: glass

hyd: hydraulic

in: inlet

ins: insulation

j: index

l: latent

o: outlet

r: room

sc: solar chimney

v: vapor

w: water

wb: wet bulb